Site and barrier energy distributions that govern the rate of hydrogen motion in quasicrystalline $Ti_{45}Zr_{38}Ni_{17}H_x$

2001 J. Phys.: Condens. Matter 13 9799

(http://iopscience.iop.org/0953-8984/13/43/310)

INSTITUTE OF PHYSICS PUBLISHING JOURNAL OF PHYSICS: CONDENSED MATTER

J. Phys.: Condens. Matter **13** (2001) 9799–9812 PII: S0953-8984(01)25712-9

Site and barrier energy distributions that govern the rate of hydrogen motion in quasicrystalline $Ti_{45}Zr_{38}Ni_{17}H_x$

A F McDowell[1,3], **Natalie L Adolphi**[1] **and C A Sholl**[2]

[1] Department of Physics, Knox College, Galesburg, IL 61401, USA
[2] Physics and Electronics, University of New England, Armidale, NSW 2351, Australia

E-mail: amcdowel@knox.edu

Received 3 July 2001
Published 12 October 2001
Online at stacks.iop.org/JPhysCM/13/9799

Abstract

The first application of a recent theory linking nuclear magnetic resonance spin–lattice relaxation rates to interstitial atom motion in disordered systems is presented. Laboratory and rotating frame relaxation rate data taken as a function of temperature for ^{1}H moving in quasicrystalline $Ti_{45}Zr_{38}Ni_{17}H_{163}$ are fitted with the new theory, yielding a hydrogen site energy distribution of Gaussian shape and width 47 ± 5 meV. The energy barriers for hydrogen motion show a Gaussian distribution of width 50 ± 5 meV, and the difference between the means of the distributions is 0.42 ± 0.01 eV. This is the first time relaxation rates have been analysed to provide information on both hydrogen site energy and barrier energy distributions simultaneously. The data are also fitted using an approach popular for disordered systems: the integration of the Bloembergen, Purcell, and Pound relaxation theory over a distribution of activation energies. The relative merits of this traditional approach and the recent theory in fitting the relaxation data, and also in fitting measurements of the static and magic angle spinning linewidths, are discussed. Although the traditional approach can fit all the data self-consistently, the theory's unsupported assumptions are undermined by the new approach.

1. Introduction

Nuclear spin–lattice relaxation rates have been reported for hydrogen nuclei in quasicrystalline $Ti_{45}Zr_{38}Ni_{17}H_x$ (Shastri *et al* 1998, 1999). Between 200 K and 550 K, motion of hydrogen between interstitial sites in the host metal structure is the dominant relaxation mechanism. The relaxation due to motion exhibits a temperature dependence similar to that observed in

[3] Author to whom any correspondence should be addressed. Office/voice mail: (309)-341-7847; laboratory: (309)-341-7826; fax: (309)-341-7718.

amorphous metal hydrides (Markert *et al* 1988, Barnes 1997). In this temperature range, the motion of hydrogen in metal hydrides is usually treated as classical over-the-barrier hopping (Grabert and Schober 1997). Hence the amorphous-like temperature dependence is not unexpected, as the complicated, albeit ordered, structure of the quasicrystal offers a variety of activation energies for the hydrogen nuclei to overcome in moving between sites. A common method for analysing such data is combining a single-activation-energy-based theory with a distribution of energy values. The most frequently chosen theory is that due to Bloembergen *et al* (1948) (referred to as BPP), which is usually combined with an assumption that the rates of motion depend on temperature through a simple Arrhenius relation. The combination is then integrated over a Gaussian distribution of activation energies. (We will refer to this traditional approach as a-BPP.) For example, Shastri *et al* (1998) used a-BPP in analysing data from a sample of quasicrystalline $Ti_{45}Zr_{38}Ni_{17}H_x$ reported to have $x = 188$, finding a mean activation energy of 0.35 eV and standard deviation of $\sigma = 0.052$ eV.

The integration of the BPP (or any other) theory over a distribution of activation energies in the traditional manner is essentially an *ad hoc* data characterization technique. There is little to physically justify this approach and the connection between the fitted parameters and the physical parameters governing the motion is not straightforward. For example, in a real material, the activation energy distribution comes from variations in both the energies of the hydrogen at interstitial sites and the energies of the barriers that must be surmounted for any particular hop to occur. The a-BPP approach makes no distinction between site and barrier energies. Recently, an alternative approach for including disorder in a BPP-based theory has been developed (Cameron and Sholl 1999a, Sholl 2000). The new approach (here referred to as CS-BPP) independently incorporates distributions of both site and barrier energies in a way that captures more of the physics of motion in disordered systems, including consideration of Fermi–Dirac statistics for site occupation probabilities and a proper calculation of the hop rate from each site. CS-BPP could also be extended to include such features as correlations between site and neighbouring barrier energies. The possibility of extracting more detailed and more physically well-founded information from relaxation data is attractive. The additional degrees of freedom should allow CS-BPP to fit the relaxation data better; the question of whether the resulting parametrization better characterizes the *motion* of the hydrogen nuclei can be addressed through measurements of motion independent of the relaxation rate measurements, such as quasi-elastic neutron scattering, pulsed-field gradient NMR, or magic angle spinning NMR (introduced below) measurements.

We present here extensive relaxation rate measurements on samples of quasicrystalline $Ti_{45}Zr_{38}Ni_{17}H_{163}$, in the temperature regime where relaxation is dominated by hydrogen motion. To further investigate the hydrogen motion, we present studies of the line narrowing of the static sample and the line broadening under magic angle spinning at two rates of sample spinning. Our main goals for this work are: to apply the CS-BPP theory in analysing actual relaxation data, to study whether the new degrees of freedom in CS-BPP allow a better fit to the data, to compare the parametrizations that result to those given by a-BPP, and to determine whether the parametrizations can legitimately be considered as descriptive of hydrogen motion. The application of CS-BPP to $Ti_{45}Zr_{38}Ni_{17}H_{163}$ provides the first characterization of both site and barrier energy distributions from spin–lattice relaxation rate data.

2. Experimental details

$Ti_{45}Zr_{38}Ni_{17}$ is a metallic icosahedral quasicrystal that can absorb large amounts of hydrogen, which enters the host lattice as individual hydrogen atoms, occupying interstitial sites without changing the lattice symmetry. The samples were prepared from elemental Ti, Zr, and Ni from

Alfa Aesar (99.95% purity), and hydrogen or deuterium was loaded from the gas phase via methods described elsewhere (Viano *et al* 1995). Powder x-ray diffraction of the hydrogenated sample, performed at the end of experimentation, showed no evidence of impurity phases (Faust *et al* 2000); narrow diffraction peaks indicated that the hydrogen was distributed uniformly throughout the sample.

The ^{1}H NMR experiments were performed using a home-built pulsed NMR spectrometer and a 2 T variable-field electromagnet with a home-built NMR field stabilizer. Sample temperatures were controlled over the range 100 K to 500 K using a home-built thermostatted flowing-gas system. Sample temperatures were measured using a copper–constantan thermocouple placed within 0.5 cm of the sample. The temperature stability was ± 1 K.

The rigid-lattice second moments (M_2) were measured using the magic echo pulse sequence (Rhim *et al* 1971, Bowman and Rhim 1982) and are described elsewhere (Faust *et al* 2000). The spin–lattice relaxation times T_1 were measured by standard inversion–recovery techniques, and the recovery curves were exponential over at least two orders of magnitude of recovery. The times T_1 were obtained at resonance frequencies of 16, 39, and 85 MHz. Spin–lattice relaxation times in the rotating frame $T_{1\rho}$ were measured (at a Larmor frequency of 85 MHz) using the standard pulse sequence (Fukushima and Roeder 1981), at rotating field strengths of 9.5 G and 29 G. The rotating field strength was determined from the π-pulse length. Pulses for nutation angle $= 10\,\pi$ were ten times longer, and no decrease in power amplifier output was observed during the long pulses of the $T_{1\rho}$-experiments. Spin–spin relaxation times T_2 were determined in three ways: at high temperatures ($T > 290$ K) T_2 was determined by measuring the height of a Hahn echo (90°–τ–180°–echo) as an exponential function of τ. At low temperatures ($T < 200$ K) T_2 was calculated from the second moment using $T_2 = (2/M_2)^{1/2}$; that is, T_2 is the $1/e$ time for the Gaussian free-induction decay (FID). In the intermediate-temperature range, we fit the FID with an exponential function. The first 4–6 microseconds of decay were distorted by amplifier recovery; a linear extrapolation from the undistorted data was used to recreate the signal at these early times. The FID was only approximately exponential, so the T_2-values for the intermediate-temperature range are not as well established as the T_2-values at higher or lower temperatures.

The ^{2}H magic angle spinning (MAS) spectra were acquired using a home-built pulsed spectrometer and a Chemagnetics variable-temperature MAS probe in a 4.7 T superconducting magnet. The powdered metal sample was mixed with an equal quantity of quartz powder to reduce eddy currents. The spectra are Fourier transforms of rotor-synchronized Hahn echoes.

3. Results and discussion

Relaxation data as a function of temperature are shown in figure 1. $Ti_{45}Zr_{38}Ni_{17}H_x$ is known to readily outgas hydrogen for $x > 1.6$, which leads to changes in T_1 (Faust *et al* 2000). Care was taken to check that T_1-values taken at the end of the entire experimental project were consistent with those taken at the beginning. We proceed by first analysing the data on the basis of a single-activation-energy theory.

The T_2^{-1}-data in figure 1 show motional narrowing of the dipole–dipole-broadened NMR line near $T = 240$ K. The onset of narrowing occurs when the correlation time is comparable to the dipolar linewidth (HWHM in rad s^{-1}): $\Delta\omega\,\tau_c = 1$ (Boden 1979). Here, the correlation time is that appropriate for the autocorrelation of the spin Hamiltonian. Spectra acquired at $T < 140$ K, well into the rigid-lattice regime, exhibited a Gaussian line with $M_2 = (1.7 \pm 0.2) \times 10^{10}$ s^{-2} (Faust *et al* 2000), from which we calculate $\Delta\omega = (1.5 \pm 0.1) \times 10^5$ rad s^{-1} and hence $\tau_c = (6.7 \pm 0.4) \times 10^{-6}$ s. We estimate the temperature of the onset by fitting the line-narrowing region with lines both above and below

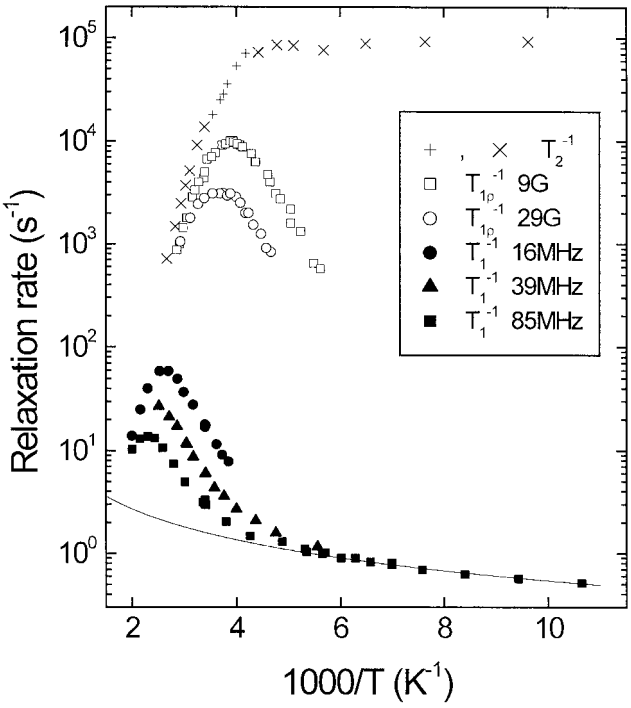

Figure 1. Relaxation rates as a function of inverse temperature for ^{1}H in an icosahedral $Ti_{45}Zr_{38}Ni_{17}H_{163}$ quasicrystal. The laboratory frame spin–lattice rates (T_1^{-1}) were measured at three resonance frequencies as shown. The rotating frame rates ($T_{1\rho}^{-1}$) were taken at two rotating field strengths, 9.5 G and 29 G. The solid line, the fit to the lowest-temperature T_1^{-1}-data, indicates the conduction electron contribution.

the narrowing temperature and determining the temperature at which the lines intersect. Some uncertainty in this procedure is due to the use of FIDs to determine T_2 at temperatures just above the onset of narrowing. The value of τ_c^{-1} at this temperature is shown in figure 2(b) along with an estimate of the uncertainties.

At low temperatures, the T_1-data in figure 1 show behaviour characteristic of the relaxation mechanism mediated by conduction electrons: $T_1T =$ constant (Korringa 1950). To focus on the relaxation mediated by hydrogen motion, the conduction electron contribution, shown as the solid line in figure 1, is subtracted from the measured rates to yield figure 2(a). The lines in figure 2(a) will be discussed below. In the BPP model with a single activation energy, T_1^{-1} and $T_{1\rho}^{-1}$ are given by

$$\frac{1}{T_1} = \frac{2}{3}M_2\left(\frac{\tau_c}{1+\omega_0^2\tau_c^2} + \frac{4\tau_c}{1+4\omega_0^2\tau_c^2}\right) \tag{1a}$$

$$\frac{1}{T_{1\rho}} = \frac{1}{3}M_2\left(\frac{3\tau_c}{1+4\omega_1^2\tau_c^2} + \frac{5\tau_c}{1+\omega_0^2\tau_c^2} + \frac{2\tau_c}{1+4\omega_0^2\tau_c^2}\right) \tag{1b}$$

with

$$\tau_c = \tau_0 \exp(E_a/k_BT). \tag{1c}$$

The T_1^{-1}-peak occurs when $\omega_0\tau_c = 0.616$, where ω_0 is the resonance frequency of the nucleus under study. Likewise, the $T_{1\rho}^{-1}$-peak occurs when $\omega_1\tau_c = 0.500$, where $\omega_1 = \gamma B_1$ is

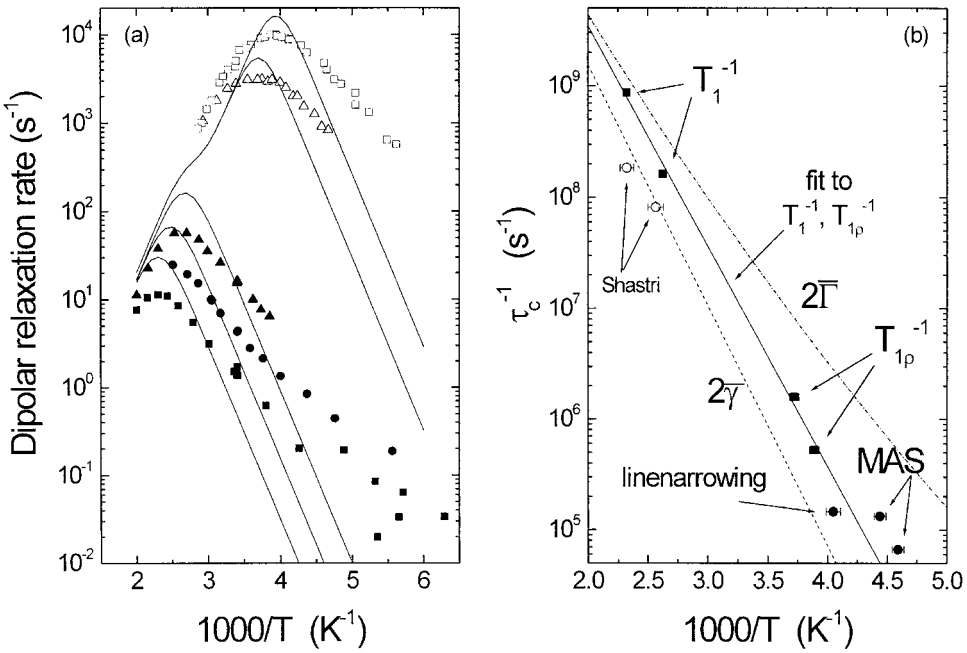

Figure 2. (a) Spin–lattice relaxation attributed to hydrogen motion. The data shown are the same data as in figure 1, with the conduction electron contribution subtracted. The lines are calculations based on the single-activation-energy BPP theory; this theory cannot account for the shapes and relative locations of the rate peaks. (b) Inverse correlation times versus temperature. The points marked T_1^{-1} and $T_{1\rho}^{-1}$ are extracted from (a) by assuming the values of $\omega\tau_c$ appropriate for BPP. The line-narrowing data point is taken from the onset of narrowing apparent in the T_2^{-1}-data in figure 1. The MAS points are from the defeat of coherent averaging demonstrated in figures 3 and 4. The solid line is a fit to the four T_1^{-1}- and $T_{1\rho}^{-1}$-points. The dotted lines labelled $2\bar{\gamma}$ and $2\bar{\Gamma}$ show the two definitions of τ_c^{-1} possible in CS-BPP, evaluated using the parameters from the fit of figure 7(b), later. The two τ_c^{-1}-values available from the work of Shastri *et al* (1998) are shown for comparison.

determined by the radio-frequency field strength. The four rate peaks in figure 2(a) therefore can be analysed to yield the correlation time at the temperature of each peak. The inverses of these τ_c-values are shown in figure 2(b), together with two points resulting from a similar analysis of the data of Shastri *et al* (1998).

Another signature of motion is provided by magic angle spinning linewidths as a function of temperature. Figure 3 shows the deuterium MAS spectrum from $Ti_{45}Zr_{38}Ni_{17}D_{160}$ for a sample spinning at 4 kHz. Deuterium was used here because the homogeneously broadened hydrogen spectrum is too broad to be narrowed by MAS; the implications of the different isotope are discussed below. The linewidth of the central line in these spectra shows a maximum as a function of temperature. This 'motional broadening' is due to random motion of the deuterium nuclei defeating the coherent averaging action of the sample spinning. Suwelack *et al* (1980) have analysed this phenomenon for the case of line broadening dominated by the chemical shift anisotropy (CSA) interaction. In their analysis, the central line (the zero-order spinning sideband) has a Lorentzian shape whose width is given by

$$\frac{1}{T_2} = \frac{1}{5}M_2\left(\frac{\tau_c}{1+4\omega_r^2\tau_c^2} + \frac{2\tau_c}{1+\omega_r^2\tau_c^2}\right) \tag{2}$$

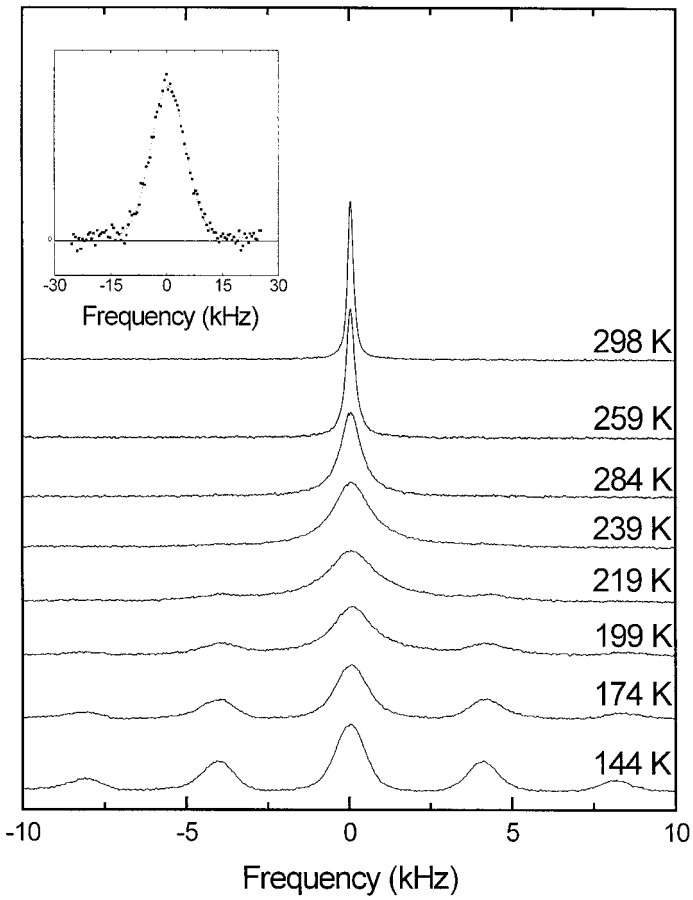

Figure 3. MAS spectra for deuterium in icosahedral $Ti_{45}Zr_{38}Ni_{17}D_{160}$ as a function of temperature. The central line ('zero-order spinning sideband') shows a maximum linewidth near 219 K. The spinning rate is 4 kHz. The inset shows the rigid-lattice, non-spinning deuterium spectrum, with a Gaussian fit.

where we have written the expression in terms of the rigid-lattice second moment, M_2, of the spectrum of the static sample. ω_r is the angular frequency of the MAS rotor. The maximum linewidth occurs when $\omega_r \tau_c = 0.893$. The peaks of the spectra shown in figure 3, as well as further data at $\omega_r/2\pi = 4$ kHz and at 8 kHz, were fitted with Lorentzians to determine the linewidth of the central peak (FWHM in rad s^{-1}, which is $1/T_2$ in the language of Suwelack *et al* 1980). The FWHM values are shown in figure 4. (The lines in the figure will be discussed below.) Aside from the spectra at the four lowest temperatures at $\omega_{rotor}/2\pi = 4$ kHz, the peaks were well fitted with Lorentzians. The spectra at the lowest three temperatures were successfully fitted with Gaussians, while the spectra at 189 K could not be fitted well with either form. For that temperature, the FWHM was determined by direct inspection of the data. All of the spectra for $\omega_{rotor}/2\pi = 8$ kHz were fitted with Lorentzians. The maximum linewidth at 4 kHz occurs at $1000/T = 4.59 \pm 0.05$ K^{-1}, where equation (2) gives the correlation time, $\tau_c = 4.2 \times 10^{-5}$ s. For deuterium, τ_c is the same as τ_D, the mean time between hops, because the dominant line-broadening interaction is between an individual deuterium nucleus and the local electric field gradient. For hydrogen $\tau_c = \tau_D/2$, because the linewidth is due to a

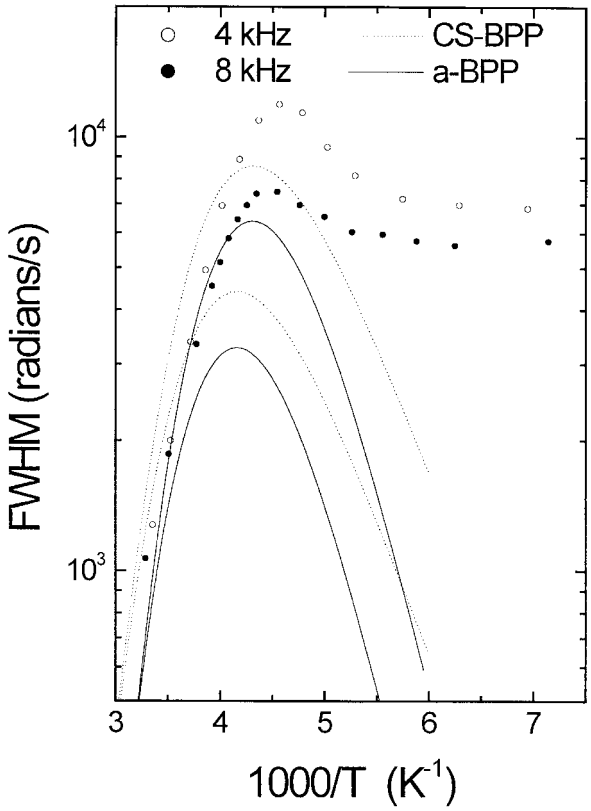

Figure 4. Summary of MAS linewidths, determined by fitting data from figure 3 and other data not shown, versus inverse temperature. Two spinning speeds, 4 kHz and 8 kHz, are shown. The uncertainties are smaller than the symbols. The solid lines are the a-BPP calculations of the linewidth, while the dashed lines are the CS-BPP calculations using the parameters from the fit of figure 7(b), later.

pairwise interaction between hydrogen nuclei, either of which may move. Hence we divide the τ_c-value derived for deuterium by two to obtain the equivalent correlation time for hydrogen τ. A further correction is needed to account for the mass difference between deuterium and hydrogen. The vibrational frequency of an atom is inversely proportional to the square root of the mass of the atom. Identifying the prefactor τ_0 with the reciprocal of this frequency requires dividing τ_c for deuterium by $\sqrt{2}$. The correlation time for hydrogen deduced from the deuterium data is therefore $\tau_c = 1.5 \times 10^{-5}$ s. For $\omega_{rotor}/2\pi = 8$ kHz we find that $\tau_c = 7.5 \times 10^{-6}$ s at $1000/T = 4.44 \pm 0.05$ K^{-1}. The inverses of the τ_c-values derived from the MAS linewidth data are shown in figure 2(b).

Figure 2(b) provides a straightforward but approximate way to compare the different manifestations of motion in the NMR data. It is important to recall that all τ_c^{-1}-values shown in figure 2(b) are based on theoretical links between motion and NMR observables, links whose validity in the presence of disorder we will probe through application of the CS-BPP approach. The τ_c^{-1}-values derived from the T_1^{-1}- and $T_{1\rho}^{-1}$-data fall on a line. The solid line in figure 2(b) is a fit of the Arrhenius relation

$$\tau_c^{-1} = \tau_0^{-1} \exp(-\bar{E}_a/k_B T) \tag{3}$$

to those points with $\bar{E}_a = 0.39 \pm 0.01$ eV and $\tau_0^{-1} = (3.2 \pm 1.5) \times 10^{13}$ s^{-1}. The prefactor, τ_0^{-1}, is of the magnitude expected, while the 'average activation energy', $\bar{E}_a$, is comparable to activation energies observed in Zr–Ti–Ni-based metal hydrides (see, for example, Richter *et al* (1992), McDowell and Cotts (1994)).

We now turn to fitting all of the relaxation rate peaks. The lines shown in figure 2(a) are an attempt to fit the peaks using the single-activation-energy BPP theory, equations (1) and (3). We have used the values of $\bar{E}_a$ and τ_0^{-1} from the solid line in figure 2(b), together with the measured value of M_2, to calculate the lines in figure 2(a). Due to the asymmetric shape and relative location of the peaks in the plot, the simple BPP theory must fail.

Following the usual a-BPP approach, we introduce a Gaussian distribution of activation energies of mean $\bar{E}_a$ and standard deviation σ and integrate equation (1) to calculate relaxation rates as a function of temperature. $\bar{E}_a$, σ, and τ_0^{-1} are adjusted to fit the data best. We find that we cannot simultaneously fit the heights of the T_1^{-1}- and $T_{1\rho}^{-1}$-data using a single value of M_2. Hence, we make two fits, one optimized to fit the T_1^{-1}-data, the other to fit the $T_{1\rho}^{-1}$-data, as shown in figure 5. The two sets of fitting parameter values are given in table 1. Note that the fitted M_2-values bracket the measured value, $(1.7 \pm 0.2) \times 10^{10}$ s^{-2}. The results of Shastri *et al* (1998), for a similar sample, $Ti_{45}Zr_{37}Ni_{17}H_{188}$, are included in the table.

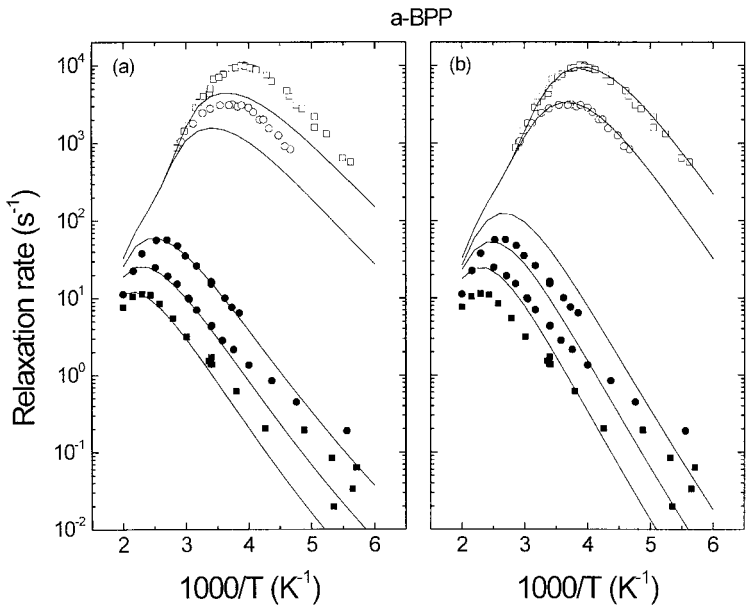

Figure 5. The a-BPP fit to the relaxation data. Panel (a) shows the optimization to the T_1^{-1}-data, while panel (b) is optimized to fit the $T_{1\rho}^{-1}$-data. The discrepancy between the two parts of the data set is not understood. The resulting parametrizations are given in table 1.

The physical source of the discrepancy between the T_1^{-1}- and $T_{1\rho}^{-1}$-data obtained from quasicrystalline $Ti_{45}Zr_{38}Ni_{17}H_{163}$ is not known. It may reflect the inadequacy of fitting the data from an ordered (albeit complicated) structure with a continuous distribution of activation energies. Our main goal is to characterize the rate of motion of hydrogen and compare the a-BPP and CS-BPP approaches. Since the choice of emphasizing the fit of either the T_1^{-1}-data or the $T_{1\rho}^{-1}$-data leads to only minor differences in the motional parameters derived, the discrepancy will not be pursued further in this paper.

Table 1. Results from a-BPP and CS-BPP fits. Separate sets of values are given for fits that were optimized to match the T_1^{-1}-data and the $T_{1\rho}^{-1}$-data.

Technique	Optimization	$\bar{E}_a$ (eV)	τ_0^{-1} (10^{13} s^{-1})	σ_{barrier} (meV)	σ_{site} (meV)	M_2 (10^{10} s^{-2})
a-BPP	$T_{1\rho}^{-1}$	0.39 ± 0.01	3 ± 1	45 ± 5[a]	45 ± 5[a]	2.1 ± 0.1
a-BPP	T_1^{-1}	0.41 ± 0.01	4 ± 1	60 ± 5[a]	60 ± 5[a]	1.1 ± 0.1
Shastri (a-BPP)	T_1^{-1}	0.35	0.6	52[a]	52[a]	1.2
CS-BPP	$T_{1\rho}^{-1}$	0.43 ± 0.01	3 ± 1	50 ± 5	50 ± 5	2.00 ± 0.05
CS-BPP	T_1^{-1}	0.41 ± 0.01	2 ± 1	50 ± 5	45 ± 5	0.86 ± 0.05
CS-BPP (barrier)	$T_{1\rho}^{-1}$	0.64 ± 0.01	2000 ± 1000	110 ± 10	0	2.66 ± 0.05
CS-BPP (barrier)	T_1^{-1}	0.64 ± 0.01	200 ± 100	120 ± 10	0	1.13 ± 0.03

[a] a-BPP does not distinguish two σ-values.

The MAS linewidth data can be fitted by convoluting the Gaussian distribution with equation (2). The results are shown by the solid lines in figure 4 for the parameters for the $T_{1\rho}^{-1}$-fit (figure 5(b)). M_2 in equation (2) is the second moment of the rigid-lattice deuterium line. The rigid-lattice (and non-spinning) deuterium spectrum is shown in the inset of figure 3, together with a Gaussian fit that yields $M_2 = (8.4 \pm 0.1) \times 10^8$ s^{-2}. (Motion of a deuterium nucleus at higher temperatures will cause its frequency to jump to different locations within this line, leading to the motional broadening analysed by Suwelack *et al* (1980). Hence we discuss the linewidth using M_2 and not the usual quadrupolar parameters.) While the lines do not match the data in figure 4, there were no free parameters available to improve the fit. The calculated linewidths reach their maxima at virtually the same temperatures as the linewidth data, and the ratio of the peak heights is reasonably well reproduced. Our experiment does not completely fit the assumptions of Suwelack *et al* (1980): an inhomogeneous broadening which can be completely overcome by MAS. The deuterium linewidth ($\approx$11 kHz FWHM) in static $Ti_{45}Zr_{38}Ni_{17}D_{160}$ is due mostly to the electric quadrupole interaction, an inhomogeneous broadening, with a small contribution (2 kHz) from magnetic dipole–dipole interactions, a homogeneous broadening. In addition, one expects a distribution of isotropic Knight shifts, which MAS does not overcome and which explains the limiting behaviour on the low-temperature side of figure 4. The variety of sources of line broadening renders the absolute size of the expected linewidths in figure 4 difficult to calculate. As implicitly assumed in our analysis of the positions of the T_1^{-1}- and $T_{1\rho}^{-1}$-peaks, we treat the temperatures of the linewidth maxima as the most salient feature in figure 4 and regard the agreement between data and calculation as satisfactory.

We are now in a position to attempt to assess figure 2(b). First, we need to address the meaning of the parameters in equation (3), which is plotted as a solid line in the figure. In general, the average hopping rate is not of Arrhenius form in disordered systems and one expects curvature in the $\log_{10}(\tau_c^{-1})$ versus $1000/T$ plot, except perhaps in special cases (Cameron and Sholl 1999b). Often, the experimentally observed curvature is small (Markert *et al* 1988). In the spirit of a-BPP, we proceed by interpreting equation (3) as giving an 'average decorrelation rate', keeping in mind that the definition of this parameter is not clearly specified. Likewise, we take $\bar{E}_a$ to be an 'average activation energy' and τ_0^{-1} to be an 'average' prefactor.

Although they lie below the solid line in figure 2(b), the two points derived from the data of Shastri *et al* are consistent with the slope (and hence average activation energy) of the line. Shastri *et al* (1998) studied a sample reported to have $x = 188$, although it is likely to have lost some of its hydrogen before the NMR measurements were made (Faust *et al* 2000). A

larger value of x will lead to a smaller τ_0^{-1} through site blocking effects, which could explain the differences between the data from these two samples.

The line-narrowing data point in figure 2(b) lies below the line, while the line-broadening (MAS) data points lie above. The discrepancy between the line narrowing and the T_1^{-1}- and $T_{1\rho}^{-1}$-data may stem in part from the difficulty in determining accurate linewidths just above the line-narrowing temperature. Furthermore, the expression $\omega_0\tau_c = 0.616$ (used to analyse the T_1^{-1}-data) is known to underestimate τ_c^{-1} in crystalline systems (Faux *et al* 1986). Studies of motion on specific lattices replace the Lorentzians in equation (1) with non-Lorentzian forms and show that the value of the constant depends on the coordination number of the hydrogen site network and the concentration of hydrogen in the material. For our sample, we expect the value to be close to 0.2, which would lead to higher τ_c^{-1}-values from the T_1^{-1}-data. The analysis of the $T_{1\rho}^{-1}$-data would have similar adjustments. These adjustments, however, are in the wrong direction to explain the discrepancy between the line narrowing and the τ_c^{-1}-values derived from T_1^{-1} and $T_{1\rho}^{-1}$ in figure 2(b). The distance between the MAS-derived τ_c^{-1}-values and the solid line may simply be due to different hydrogen (deuterium) concentrations in the two samples. Furthermore, our MAS experiment does not fully satisfy the assumptions underlying equation (2), as we have discussed above. Finally, an application of the work of Faux *et al* (1986) to equation (2) would presumably modify the constant value in $\omega_r\tau_c = 0.893$, as discussed for the T_1^{-1}- and $T_{1\rho}^{-1}$-data. Given these caveats, we find the agreement between the T_2^{-1}-derived and MAS-derived τ_c^{-1}-values and the line fit to the values derived from T_1^{-1} and $T_{1\rho}^{-1}$ satisfactory; the a-BPP approach can self-consistently fit the NMR data reasonably well.

However, internal consistency is not enough to show that a-BPP leads to physically relevant parametrizations. We now use CS-BPP to generate an alternative, more detailed, and more physically well-founded parametrization of hydrogen motion. In figure 6 we show the fit of

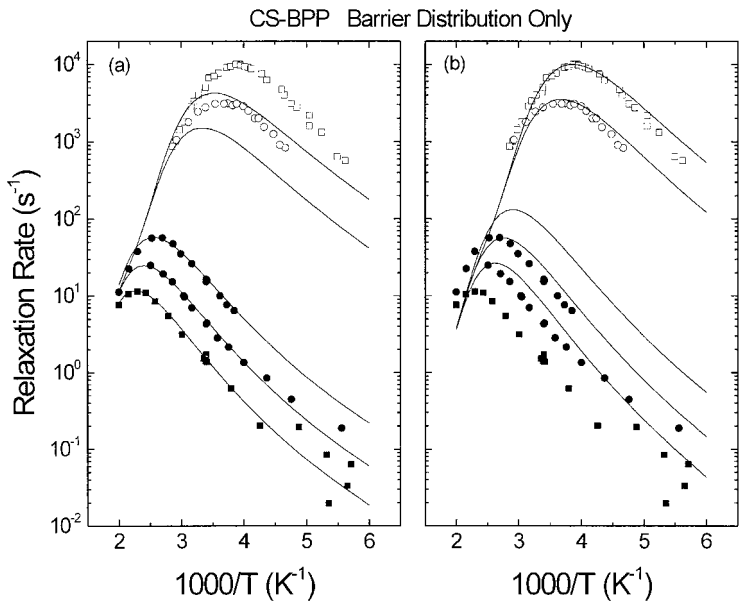

Figure 6. The partial CS-BPP fit, with identical site energies and distributed barrier energies. Again, the two panels show the fit optimized to either T_1^{-1}- or $T_{1\rho}^{-1}$-data, with both parametrizations given in table 1. Here, the fits are such that optimization to one data type leads to errors in fitting the temperatures of the other peaks.

the CS-BPP theory which includes a Gaussian distribution of barrier energies but only a single value of the site energy. In figure 6(a), the fit is optimized to the T_1^{-1}-data, while in figure 6(b) the fit is optimized to the $T_{1\rho}^{-1}$-data. Both parametrizations are given in table 1. The M_2-values that result bracket the measured value, and the 'average activation energy', defined as the difference between the average energy of the barrier distribution and the site energy, is the same for both optimizations. The fit to the T_1^{-1}-data is superior to the fit generated by a-BPP, while the fit to the $T_{1\rho}^{-1}$-data is somewhat worse. Note, however, that when the fit is optimized to one set of peaks, the others fail to match the data not only in height, but also in temperature. This temperature error is a manifestation of the order-of-magnitude difference in τ_0^{-1} for the two optimizations. The CS-BPP with only a barrier distribution is not conclusively better at fitting the NMR data. However, the fact that this physically better grounded theory gives an 'average activation energy' radically different from a-BPP raises a serious challenge to the a-BPP approach. The partial CS-BPP approach, with only a barrier distribution, eliminates the importance of Fermi–Dirac statistics and maps very simply onto the distribution in the a-BPP method. The disagreement between these approaches stems from the different ways in which they incorporate the physics of motion on a disordered potential surface. Given the disagreement, it is not clear that a-BPP gives reliable information about the potential energy surface experienced by the hydrogen atoms.

In figure 7 we show the full CS-BPP theory, with independent Gaussian distributions in both site and barrier energies, fitted to the relaxation rate peaks. As for figure 6, the two panels show the two optimizations and the parameters are given in table 1. The value of $\bar{E}_a$ is the difference between the mean barrier energy and the mean site energy. The value of τ_0^{-1} is twice the prefactor for the jump rate of a single spin between sites and is assumed to be the same for all sites. This definition of τ_0^{-1} is consistent with equation (3). The only

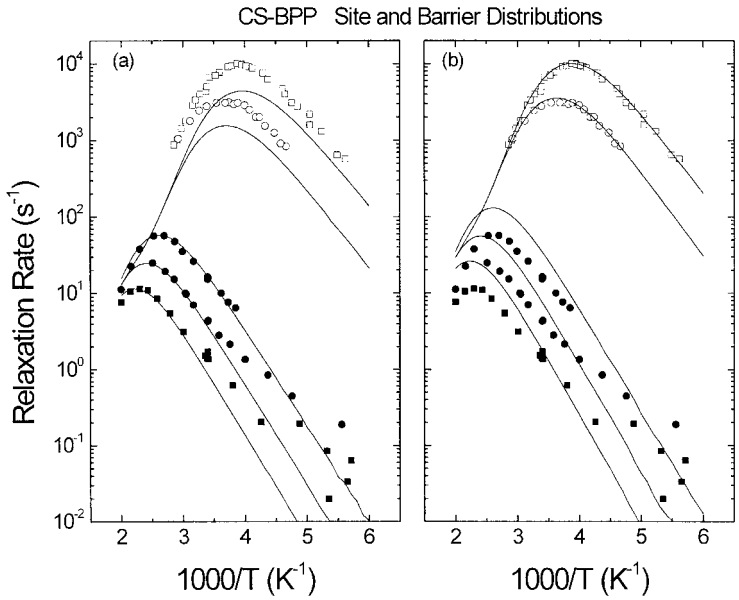

Figure 7. The full CS-BPP fit, with distributions of both site and barrier energies. Again, the two panels show the fit optimized to either T_1^{-1}- or $T_{1\rho}^{-1}$-data, with both parametrizations given in table 1. Optimizations to either data type still give relatively accurate fits to the temperatures of the other peaks.

significant difference between these two parametrizations is in their effective M_2-values, which is manifested graphically by the fact that when the fit is optimized to one set of peaks, the other set appear at the right temperatures (and with the right shapes); only the heights of the other peaks are incorrect. The parameters are consistent with the a-BPP results, and with CS-BPP one can attribute the source of the a-BPP parameters to an equal level of disorder in the site and barrier energies. This is the first time that such a direct connection between the disorder apparent in the shapes of the NMR relaxation peaks and disorder in the potential energy surface experienced by the moving atoms has been made.

We show the CS-BPP calculations of the MAS linewidths as the dotted lines in figure 4. Here, the parameters from the fit of figure 7(b) were used, together with the measured value of M_2. Hence, there are no free parameters. We interpret the level of agreement with the data as satisfactory given the above discussion of figure 4.

In a simple ordered system with a single jump rate, τ_c^{-1} can be interpreted as twice the jump rate of a diffusing spin. In disordered systems, the discussion of the temperature dependence of τ_c^{-1} (as displayed in figure 2(b)) must be approached with care. There are at least two possible interpretations for τ_c^{-1}:

(i) as twice the jump rate defined by the difference between the average site energy and average barrier energy (denoted as $\bar{\gamma}$ by Cameron and Sholl 1999b) and
(ii) as twice the true average jump rate (denoted as $\bar{\Gamma}$).

$\bar{\gamma}$ and $\bar{\Gamma}$ are not equal, due to the (temperature-dependent) weighting effects of Fermi–Dirac occupation statistics and of competing jump paths from individual sites. The a-BPP theory contains no basis on which to distinguish between these two possibilities, which leaves equation (3) without a clear physical interpretation.

In figure 2(b), we plot $2\bar{\gamma}$ and $2\bar{\Gamma}$ for the parameters of the full CS-BPP fit to the $T_{1\rho}^{-1}$-data (figure 7(b)). $2\bar{\gamma}$ is, by definition, of Arrhenius form and reflects the 'average activation energy'. $2\bar{\Gamma}$ is twice the true average hop rate and does *not* have the Arrhenius temperature dependence. Comparison to the data points in figure 2(b) is not straightforward. The τ_c^{-1}-values derived from the peaks in the relaxation data and from MAS linewidth maxima are based on an unsupported assumption (constancy of values of the product $\omega\tau_c$) and a poorly defined τ_c^{-1}. The τ_c^{-1} derived from line narrowing may be expected to be more robust, as the link between motion and the NMR observable is based on averaging over possible resonance frequencies. This is considerably more straightforward than the link between motion and relaxation, which involves assumptions about the forms of the spectra of Hamiltonian fluctuations. The $2\bar{\gamma}$ line passes fairly close to the line-narrowing-derived τ_c^{-1}-point, while the $2\bar{\Gamma}$ line passes well above the point. One might expect that the true average jump rate ($\bar{\Gamma}$) would have been more directly relevant to the line narrowing. Further theoretical work is required to firmly establish line narrowing as a measure of τ_c^{-1} for disordered systems. A complete test of the CS-BPP parametrization will require an independent determination of τ_c^{-1}, perhaps through neutron scattering or pulsed field gradient NMR measurements of diffusion. Such a determination is not currently available.

Within the CS-BPP theory, it is possible to test the validity of the assumption of constancy of the product $\omega\tau_c$. While valid for an ordered system, this assumption has no physical justification for disordered materials, and there is evidence that it is incorrect (McDowell 1993, Cameron and Sholl 1999a). Taking $\tau_c^{-1} = 2\bar{\gamma}$ (with parameters from the $T_{1\rho}^{-1}$-optimized fit of figure 7(b)), we find $\omega_0\tau_c = 1.05$, 1.1, and 1.2 for the T_1^{-1}-peaks at 85, 39, and 16 MHz, respectively. For the two $T_{1\rho}^{-1}$-peaks, we find $\omega_1\tau_c = 1.6$ and 1.9 for the peaks at 9.5 G and 29 G, respectively. These values are 2 to 4 times larger than the values taken from BPP, and not quite constant. Figure 2(b) demonstrates the non-constancy through the lack of parallelism

between the solid line (based on the products $\omega\tau$) and the dashed $2\bar{\gamma}$ line. One can readily see that the values of $\omega\tau_c$ derived from the definition $\tau_c^{-1} = 2\bar{\Gamma}$ will be *smaller* than BPP values, and even more strongly varying. Clearly, the CS-BPP results undermine the assumption of constant values of $\omega\tau$. In contrast to the a-BPP theory, the parameters in the CS-BPP theory are well defined within the model and therefore provide a direct connection to the energy disorder and the jump rate parameters of diffusing spins.

4. Conclusions

The advent of a new BPP-based data analysis methodology, CS-BPP, has allowed us to test the validity of more traditional BPP and a-BPP approaches for disordered systems. Using ^{1}H relaxation data from an icosahedral $Ti_{45}Zr_{38}Ni_{17}H_{163}$ quasicrystal as a test case, we have applied the BPP, a-BPP, partial CS-BPP, and full CS-BPP schemes. Despite the relatively good fits, there are considerable grounds for concern that the parametrizations of a-BPP do not directly characterize the microscopic physics of interstitial motion in disordered (or complicated) host materials.

The partial CS-BPP application, in which site energies were all identical and only barrier energies were distributed, produced an 'average activation energy' more than 50% larger than for a-BPP. The fit quality is comparable and so provides no discrimination between analysis techniques. The superior physical foundation of CS-BPP leads one to favour its parametrization, since the parameters can be directly assigned to features of the potential energy surface. The relevance of the a-BPP parametrization as a characterization of this energy surface is called into question.

Fits of a similar quality are achieved with a full implementation of CS-BPP, which provides separate, simultaneous characterizations of the site and barrier energy distributions. For our particular sample, the 'average activation energy' for full CS-BPP agrees well with a-BPP, although it is not known whether this will always be the case. The CS-BPP fits shown demonstrate that the technique is practical and computationally tractable.

Finally, with a well-defined correlation time, it is possible to show that the usual assumption of constancy of the values of the product $\omega\tau$ values fails for disordered systems.

Acknowledgments

AFM and NLA thank the NSF for support under grant DMR 9804094 and Ann Viano and Jae Kim for samples. NLA thanks the Research Corporation for support under grant CC4705.

References

Barnes R G 1997 *Top. Appl. Phys.* **73** 93
Bloembergen N, Purcell E M and Pound R V 1948 *Phys. Rev.* **73** 679
Boden N 1979 *The Plastically Crystalline State* ed J N Sherwood (New York: Wiley)
Bowman R C Jr and Rhim W-K 1982 *J. Magn. Reson.* **49** 93
Cameron L M and Sholl C A 1999a *J. Alloys Compounds* **293–295** 260
Cameron L M and Sholl C A 1999b *J. Phys.: Condens. Matter* **11** 4491
Faust K R, Pfitsch D W, Stojanovich N A, McDowell A F, Adolphi N A, Majzoub E H, Kim J Y, Gibbons P C and Kelton K F 2000 *Phys. Rev.* B **62** 11 444
Faux D A, Ross D K and Sholl C A 1986 *J. Phys. C: Solid State Phys.* **19** 4115
Fukushima E and Roeder S B W 1981 *Experimental Pulsed NMR* (London: Addison-Wesley)
Grabert H and Schober H R 1997 *Top. Appl. Phys.* **73** 5
Korringa J 1950 *Physica* **16** 601

Markert J T, Cotts E J and Cotts R M 1988 *Phys. Rev.* B **37** 6446
McDowell A F 1993 *PhD Thesis* Cornell University, NY
McDowell A F and Cotts R M 1994 *Z. Phys. Chem.* **183** 65
Rhim W-K, Pines A and Waugh J S 1971 *Phys. Rev.* B **3** 684
Richter D, Hempelmann R and Bowman R C Jr 1992 *Hydrogen in Intermetallic Compounds II* ed L Schlapbach (Berlin: Springer)
Shastri A, Majzoub E H, Borsa F, Gibbons P C and Kelton K F 1998 *Phys. Rev.* B **57** 5148
Shastri A, Majzoub E H, Borsa F, Gibbons P C and Kelton K F 1999 *Phys. Rev.* B **59** 14 108
Sholl C A 2000 *J. Phys.: Condens. Matter* **12** 4285
Suwelack D, Rothwell W P and Waugh J S 1980 *J. Chem. Phys.* **73** 2559
Viano A M, Stroud R M, Gibbons P C, McDowell A F, Conradi M S and Kelton K F 1995 *Phys. Rev.* B **51** 12 026